Width of the charge-transfer peak in the SU(N) impurity Anderson model and its relevance to nonequilibrium transport

J. Fernández,[1] F. Lisandrini,[2] P. Roura-Bas,[3] C. Gazza,[2] and A. A. Aligia[1]

[1]*Centro Atómico Bariloche and Instituto Balseiro, Comisión Nacional de Energía Atómica, CONICET, 8400 Bariloche, Argentina*

[2]*Instituto de Física Rosario. Facultad de Ciencias Exactas Ingeniería y Agrimensura, Universidad Nacional de Rosario. Bv. 27 de Febrero 210 bis, 2000 Rosario, Argentina*

[3]*Dpto de Física, Centro Atómico Constituyentes, Comisión Nacional de Energía Atómica, CONICET, Buenos Aires, Argentina*

(Received 7 September 2017; revised manuscript received 17 January 2018; published 25 January 2018)

We calculate the width $2\Delta_{\rm CT}$ and intensity of the charge-transfer peak (the one lying at the on-site energy E_d) in the impurity spectral density of states as a function of E_d in the SU(N) impurity Anderson model (IAM). We use the dynamical density-matrix renormalization group (DDMRG) and the noncrossing approximation (NCA) for $N = 4$ and a $1/N$ variational approximation in the general case. In particular, while for $E_d \gg \Delta$, where Δ is the resonant level half-width, $\Delta_{\rm CT} = \Delta$ as expected in the noninteracting case, for $-E_d \gg N\Delta$ one has $\Delta_{\rm CT} = N\Delta$. In the $N = 2$ case, some effects of the variation of $\Delta_{\rm CT}$ with E_d were observed in the conductance through a quantum dot connected asymmetrically to conducting leads at finite bias [J. Könemann *et al.*, Phys. Rev. B **73**, 033313 (2006)]. More dramatic effects are expected in similar experiments that can be carried out in systems of two quantum dots, carbon nanotubes or other, realizing the SU(4) IAM.

DOI: 10.1103/PhysRevB.97.045144

I. INTRODUCTION

The discovery of the Kondo effect [1] in semiconducting quantum dots (QDs) [2–10] has spurred the study of electronic transport through QDs. Later molecular QDs [11–21], and QDs in carbon nanotubes [22–24], were also studied. Molecular QDs in general have large asymmetric coupling to source and drain leads. Semiconducting QDs are characterized by the enormous possibilities for tuning the different parameters. In all these systems, several physical effects are generically observed when the system is cooled at cryogenic temperatures due to the large Coulomb repulsion in these nanoscopic QDs, such as Coulomb blockade and the Kondo effect, which implies a resonance at the Fermi energy in the spectral density of the dot state that leads to an anomalous peak in the differential conductance $G(V) = dI/dV$ at zero bias voltage V, where I is the current through the QD. These physical effects are usually well described by an impurity Anderson model (IAM).

While intense research has been devoted to the Kondo effect, also important effects of the interactions take place at finite V that are unexpected for independent electrons. In particular, Coulomb blockade peaks were shown to present a strong width renormalization in the situation of large tunnel asymmetries between source and drain electrodes [25]. Specifically, K önemann *et al.* started from an equilibrium situation in which the dot level $E_d > 0$. Then they applied a bias voltage, which shifts the chemical potential μ_L of one of the leads (we call it the left lead) in $eV > 0$ and also E_d by about $eV/2$ due to capacitance effects. A peak in $G(V)$ is observed when $\mu_L \sim E_d$. When instead a bias voltage such that $eV < 0$ is applied, another peak in $G(V)$ was observed (when $E_d \sim \mu_R$, the chemical potential of the right lead). In a noninteracting picture, one would expect that both peaks have nearly the same width and the same height [26,27]. However, the latter turns out to be about two times wider and with a maximum nearly five times smaller [25]. The reason is that the QD has a much stronger coupling to the right lead, and then for $eV > 0$ the QD is empty, while for $eV < 0$ it is in an intermediate valence situation, and one knows that the half width at half maximum $\Delta_{\rm CT}$ of the spectral density of the charge-transfer (CT) peak in the IAM increases with the occupancy [27–29]. An explanation of the experiment in the framework of the SU(2) IAM, including the effects of capacitance and tunneling asymmetries and the Kondo effect is provided in Ref. [27].

Several tunable systems of the kind discussed above in which there is an orbital, dot, or valley degeneracy, in addition to the spin one, are described by the SU(4) IAM, like those of carbon nanotubes [22–24], a nanoscale Si transistor [30], an As dopant in a Si nanostructure [31], and systems of two QDs where the occupation of one or the other QD plays the role of the orbital degeneracy [9,10]. In the latter case, the tunneling coupling of both dots are in general different, reducing the symmetry to SU(2), but tuning other parameters the SU(4) symmetry can be recovered as an emergent one at low temperatures [32,33]. Crossovers [30,34–40] and abrupt transitions [41] between SU(2) and SU(4) symmetry were also studied.

In the noninteracting case, for a flat very wide conduction band as we assume, the spectral density of the localized level for each of the N components in the SU(N) impurity Anderson model is a Lorentzian with half width at half maximum Δ [defined by Eq. (2) in terms of the microscopic parameters of the model]. Thus in this case, $\Delta_{\rm CT} = \Delta$ independently of on-site energy E_d. As we show in this paper, the effect of correlations on $\Delta_{\rm CT}$ increases with N and one expects a width $\Delta_{\rm CT} = N\Delta$ for the SU(N) model in the Kondo regime $-E_d, E_d + U \gg \Delta$, where U is the Coulomb repulsion. Therefore if the experiments like those of Könemann *et al.* are performed for any of the above realizations of the SU(4) IAM, this effect would be more evident. Furthermore for the experiments with the setup

of two QDs in which each QD is connected to its own pair of conducting leads and the tunneling matrix elements and the voltages at the four leads can be controlled independently with high precision [8,10], the spectral density can be read out directly from the differential conductance through one of the QD under appropriate conditions [39].

In this paper we use a $1/N$ expansion based on variational wave functions [42,43], to show that one expects in general that $\Delta_{\rm CT} \sim N\Delta$ for $-E_d \gg N\Delta$ in the SU(N) IAM. We also calculate $\Delta_{\rm CT}$ as a function of E_d for $N = 4$ using dynamical density-matrix renormalization group (DDMRG) and the noncrossing approximation (NCA). In this case $\Delta_{\rm CT}$ changes rather abruptly from 4Δ to Δ as the effective E_d (including renormalization due to effects of the hybridization [44]) changes sign from negative to positive. We also discuss the possible experimental relevance of these results.

The paper is organized as follows. In Sec. II, we describe the SU(N) IAM and the methods used. In Sec. III we discuss the CT peak for general N at zero temperature in the Kondo regime $-E_d \gg N\Delta$ using a variational approximation. Section IV contains NCA and DDMRG results for $N = 4$. In Sec. V we show the results for the occupancy as a function of on-site energy level and compare them with the noninteracting case and with exact Bethe ansatz results. In Sec. VI we discuss the relevance of our results to possible experimental realizations. Section VII contains a summary and a discussion.

II. MODEL AND METHODS

We consider the one-level SU(N) IAM with infinite on-site repulsion U. The impurity states involve a singlet configuration $|s\rangle$ together with a degenerate configuration $|m\rangle$, $m = 1$ to N, corresponding to one additional electron (or hole) in the "impurity," which can be a QD, a system of two QDs, a part of a carbon nanotube, or an atom with degenerate levels as discussed in the introduction. When discussing transport experiments, for simplicity we assume that the "impurity" is connected to a left (L) and a right (R) conducting lead. An extension to the case of the system of two QDs in which both are connected to a pair of independent leads [8–10] is straightforward [39]. The Hamiltonian reads:

$$H = \sum_m E_d |m\rangle\langle m| + \sum_{\nu k m} \epsilon_{\nu k} c^\dagger_{\nu k m} c_{\nu k m} + \sum_{\nu k m} (V^\nu_k |m\rangle\langle s| c_{\nu k m} + \text{H.c.}), \quad (1)$$

where the constraint $|s\rangle\langle s| + \sum_m |m\rangle\langle m| = 1$ is imposed (this is equivalent to the assumption of infinite Coulomb repulsion U). Here $c^\dagger_{\nu k m}$ create conduction states in the lead ν with projection m and wave vector k. The tunnel couplings of the quantum dot to the leads and the total resonant level widths are

$$\Delta_\nu = \pi \sum_k \left|V^\nu_k\right|^2 \delta(\omega - \epsilon_{\nu k}),$$
$$\Delta = \Delta_L + \Delta_R \quad (2)$$

taken in general independent of energy ω [45]. For the discussion of the impurity spectral density $\rho_m(\omega)$, only Δ is relevant.

To obtain $\rho_m(\omega)$ we use three different methods. The variational one, based on Refs. [42,43] is the simplest one and is described in detail in the next section. It is limited to the Kondo regime $-E_d \gg N\Delta$ and zero temperature. We also use NCA and DDMRG.

The NCA is equivalent to a sum of an infinite series of diagrams in perturbations in the hybridization [1,46,47]. In the Kondo regime, it is known to reproduce correctly the relevant energy scale T_K and its dependence of parameters. An advantage for our purpose over the numerical-renormalization group in which finite-energy features are artificially broadened due to the logarithmic discretization of the conducting band [48,49], NCA correctly describes these features. For instance, the NCA works satisfactorily in cases in which the conduction density of states is not smooth [47], including in particular a step in the conduction band [50]. Furthermore, it has a natural extension to nonequilibrium conditions [51], and it is specially suitable for describing satellite peaks of the Kondo resonance, as those observed in Ce systems [52,53], or away from zero bias voltage in nonequilibrium transport due to phonons [54,55] or magnetic and orbital excitations [32,56,57]. Alternatives to NCA for nonequilibrium problems are renormalized perturbation theory (but limited to small ω, V and temperature T) [58–60] or the equation of motion method [61,62], although it does not reproduce correctly the functional dependence of T_K on E_d [62,63].

However, the NCA has important limitations out of the Kondo regime. In particular for moderate positive E_d, the impurity self energy has an unphysical positive imaginary part (this means that the Green function violates causality) and the impurity spectral density presents a spurious peak at the Fermi energy. As a consequence, the NCA results in this region of E_d are unreliable. For this reason, we also use the DDMRG in its correction-vector-method approach. Since it was introduced by Kuehner and White [64], the correction vector has shown to be a reliable way to do dynamical calculations with DMRG in different low-dimensional strongly correlated models. Different strategies were done to include the correction vector in the target states of a standard DDMRG [65–67]. We choose a recently presented version introduced by Nocera and Alvarez [68], which based on a Krylov-space approach has been shown to be more accurate and efficient than conjugate gradient [67].

However, the two major difficulties of the correction-vector method persist. First, the need to be computed in small frequency intervals which is unavoidable but with parallelization strategies becomes affordable. Second the artificial broadening η that is necessarily introduced in the calculation (calculations cannot be done at $\eta = 0$). Therefore one is computing $G(\omega + i\eta)$, and the resulting impurity density spectral function $\rho^{(\eta)}(\omega) = -\frac{1}{\pi}\text{Im}G(\omega + i\eta)$ can be visualized as the real spectral density $\rho(\omega)$ convoluted by the Lorentzian $\rho_d(\omega) = (\eta/\pi)/((\omega - \omega_0)^2 + \eta^2)$ of width η. Since we are interested in the real spectral density for $\eta \to 0^+$, this compels to a deconvolution of the spectrum, and many proposals have been presented to do this difficult task successfully [69–75] and resolve structures with small width in the real spectrum. Fortunately, as it was mentioned above, we are interested in the line shapes of the CT peak for the IAM which as it has been very well described in Ref. [74], the deconvolution becomes easiest, par-

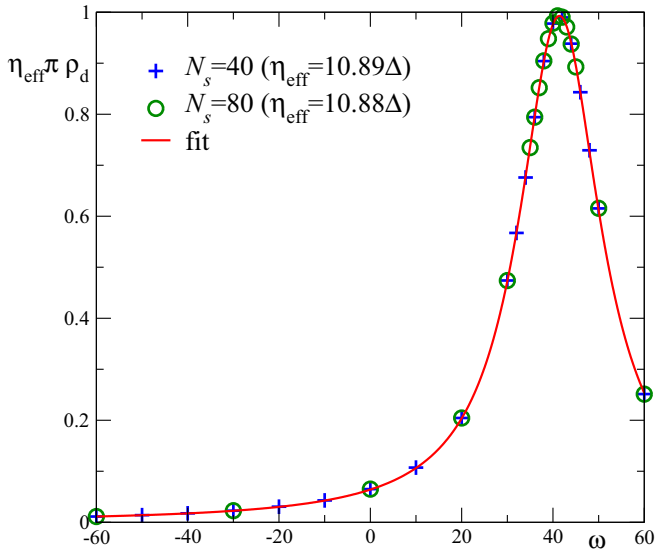

FIG. 1. DDMRG correction vector data of the CT at $\eta = 10\Delta$. Open circles (crosses) for $N_s = 40$ ($N_s = 80$), for $E_d = 40\Delta$ (see Fig. 3). In legends we indicate the $\eta_{\rm eff}$ obtained from a fit with a Lorentzian $\propto K/((\omega-\omega_{up})^2+\eta_{\rm eff}^2)$ (thin line) for each size.

ticularly for large U. The authors have also shown that the noninteracting case $U = 0$ is well described by the DDMRG [74].

Assuming that the original CT peak is a Lorentzian, then the data obtained with DDMRG will be the convolution of two Lorentzians of half width at half maximum $\Delta_{\rm CT}$ and η, respectively. This convolution will result in a new Lorentzian whose half width is the sum of the two original ones, so that the half width at half maximum of the peak obtained by fitting the DDMRG calculations will be $\eta_{\rm eff} = \Delta_{\rm CT} + \eta$. The strategy works fine while the CT peak does not merge with the Kondo peak, obtaining reliable results in the range $E_d \geqslant 10\Delta$. When both peaks overlap, we still can distinguish the left part of the CT (at lower frequencies) and we fit just the left half part of CT peak using the DDMRG data. Calculations were done with up to 1000 states keeping the truncation error less than 10^{-8}, assuring a numerical error in DDMRG data much smaller than the size of the symbols in Fig. 1.

In order to visualize the procedure, we show in Fig. 1 the DDMRG correction vector results, for $E_d = 40\Delta$ with $\eta = 10\Delta$, and for two sizes ($N_s = 40$, 80). As is apparent in the figure, there are no significant finite-size effects. Then we fit the peaks with Lorentzians to obtain the half width $\eta_{\rm eff}$ and the position $E_d^{\rm eff}$ for each lattice size, allowing us to take the estimation $\eta_{\rm eff} = (10.9 \pm 0.1)\Delta$. Finally we can calculate the values presented in Fig. 3 doing the subtraction of the width obtained with the $\eta = 10\Delta$ used in the correction vector. We derive in our example $\Delta_{\rm CT} = (0.9 \pm 0.1)\Delta$.

III. WIDTH AND WEIGHT OF THE CHARGE-TRANSFER PEAK FOR LARGE NEGATIVE ON-SITE ENERGY

In this section we calculate $\Delta_{\rm CT}$ well inside the Kondo regime $-E_d \gg N\Delta$, using a variational procedure [42,43]. The ground-state wave function of the Hamiltonian Eq. (1) is approximated as

$$|g\rangle = A|F\rangle + \sum_{qm} B_q d_m^\dagger c_{qm}|F\rangle, \tag{3}$$

where $|F\rangle = \Pi'_q c^\dagger_{qm}|0\rangle \bigotimes |s\rangle$ is the state with the filled Fermi sea in the band and the impurity in the singlet state, the subscript q refers to both lead and wave vector index [ν and k in Eq. (1)], the prime over the product symbol means that only q for which $\epsilon_q < \epsilon_F$ are included, where ϵ_F is the Fermi energy. We denote $d_m^\dagger = |m\rangle\langle s|$. The variational parameters A and B_q are determined minimizing the energy. The B_q are independent of m as a consequence of SU(N) symmetry. Normalization of $|g\rangle$ implies

$$|A|^2 + N\sum_q |B_q|^2 = 1. \tag{4}$$

In the following we take the origin of energies at the Fermi energy $\epsilon_F = 0$. We define the energy gain due to hybridization as

$$T_K = E - E_0, \tag{5}$$

where E is the ground-state energy and $E_0 = E_d + \langle F|H|F\rangle$, the ground-state energy for $V_q = 0$. Minimizing the energy one obtains

$$B_q = \frac{-\bar{V}_q A}{T_K - \epsilon_q}, \tag{6}$$

and the equation for the ground-state energy, which can be written in the form

$$T_K - E_d - N\sum_q \frac{|V_q|^2}{T_K - \epsilon_q} = 0. \tag{7}$$

The sum can be evaluated assuming $\Delta = \Delta_L + \Delta_R = \pi\sum_q |V_q|^2\delta(\omega-\epsilon_q)$ independent of ω in the range $-D < \omega < D$ and gives $(\Delta/\pi)\ln[(D+T_K)/T_K]$. In the Kondo limit $-E_d \gg N\Delta$, one can neglect T_K in comparison with D and $|E_d|$ obtaining

$$T_K = D\exp\left(\frac{\pi E_d}{N\Delta}\right), \tag{8}$$

which has the correct exponential dependence on E_d (although the correct prefactor is smaller [1,76]).

At zero temperature, the impurity spectral density is

$$\begin{aligned}\rho_m(\omega) &= \rho_m^d(\omega) + \rho_m^c(\omega),\\ \rho_m^d(\omega) &= \sum_e |\langle e|d_m|g\rangle|^2\delta(\omega + E_e - E),\\ \rho_m^c(\omega) &= \sum_e |\langle e|d_m^\dagger|g\rangle|^2\delta(\omega - E_e + E),\end{aligned} \tag{9}$$

where E_e is the energy of the excited state $|e\rangle$. Since we are interested in ω near E_d and in this section E_d is well below the Fermi energy, we can neglect the creation part $\rho_m^c(\omega)$ of the spectral density. Using Eq. (3) we can write

$$\begin{aligned}\rho_m^d(\omega) &= -\frac{1}{\pi}\sum_q |B_q|^2 {\rm Im}G_{qm,qm}(E-\omega),\\ G_{qm,qm}(z) &= \langle qm|\hat{G}|qm\rangle,\ |qm\rangle = c_{qm}|F\rangle,\\ \hat{G}(z) &= \frac{1}{z + i\eta - H},\end{aligned} \tag{10}$$

where $\eta \to 0^+$ is a positive infinitesimal.

Defining the operators $\hat{G}^0(z) = z + i\eta - H_0$, where $H_0 = H - \hat{V}$, and $\hat{V} = \sum_{qm}(V_q d_m^\dagger c_{qm} + \text{H.c.})$ is the hybridization part of H, one has the Dyson equation

$$\hat{G} = \hat{G}^0 + \hat{G}^0 \hat{V} \hat{G}. \tag{11}$$

Taking matrix elements of both members Eq. (11) between states $|qm\rangle$ and/or $|q'm'qm\rangle = d_{m'}^\dagger c_{q'm'}|qm\rangle$, we obtain after some algebra

$$\begin{aligned} &G_{qm,qm}(z) \\ &= \frac{G^0_{qm,qm}(z)}{1 - G^0_{qm,qm}(z)\sum_{q'm'}|V_{q'}|^2 G^0_{q'm'qm,q'm'qm}(z)}, \\ &G^0_{qm,qm}(z) = \frac{1}{z + i\eta + \epsilon_q - E_0 + E_d}, \\ &G^0_{q'm'qm,q'm'qm}(z) = \frac{1}{z + i\eta + \epsilon_q + \epsilon_{q'} - E_0}. \end{aligned} \tag{12}$$

The sum over m' above is just a factor N due to SU(N) symmetry. As we shall see, this factor enters into the width of the charge-transfer (CT) peak Δ_{CT}. The sum over q' can be evaluated using the density of conduction states [as we have done to obtain Eq. (8)], leading to

$$\begin{aligned} \text{Im}G_{qm,qm}(E-\omega) &= \frac{-N\Delta}{\left(\omega + T_K - \epsilon_q - E_d - \Lambda\right)^2 + (N\Delta)^2}, \\ \Lambda &= \frac{N\Delta}{\pi} \ln\left|\frac{D + \omega + T_K - \epsilon_q}{\omega + T_K - \epsilon_q}\right|. \end{aligned} \tag{13}$$

Inserting this in the first Eq. (10) and using Eqs. (4) and (6) one obtains the desired spectral density.

In the limit $-E_d \gg N\Delta, T_K$ becomes exponentially small [see Eq. (8)]. Furthermore, from Eq. (6), one realizes that the values of ϵ_q which lead to the larger values of $B_q \sim A/T_K$ are of the order of T_K. From Eqs. (4) and (6) one sees that for $T_K \to 0$, also $A \to 0$ and $\sum_q |B_q|^2 \to 1/N$. Thus in this limit $T_K \to 0$, for any function $F(\epsilon_q)$, we can use

$$\sum_q |B_q|^2 F(\epsilon_q) \to \frac{1}{N} F(0). \tag{14}$$

Furthermore since Λ has a weak logarithmic dependence and we are interested in $\omega \sim E_d$, we can evaluate it at E_d. Then Eqs. (13), the first (10) and (14) lead to

$$\rho_m(\omega) \simeq \frac{\Delta/\pi}{\left(\omega - E_d^{\text{eff}}\right)^2 + (N\Delta)^2}, \tag{15}$$

$$E_d^{\text{eff}} = E_d + \frac{N\Delta}{\pi} \ln\left|\frac{D + E_d}{E_d}\right|, \tag{16}$$

well inside the Kondo limit $-E_d \gg N\Delta$.

This simple result reflects three important physical effects of the correlations on the CT peak: (i) The position is shifted upwards. The origin of this shift was explained by Haldane for the SU(2) case [44], and extensions to the SU(4) case and the SU(2) $\leftrightarrow$ SU(4) crossover were discussed [32,76]. Depending on details different but similar estimations for the shift were given. This point is discussed in more detail in Sec. IV A (see Fig. 4). (ii) The half width at half maximum of the peak is $\Delta_{\text{CT}} = N\Delta$. This is a factor N with respect to the noninteracting case. (iii) The total weight of the peak is $1/N$. The maximum intensity is thus reduced in a factor $1/N^2$ compared to the noninteracting case.

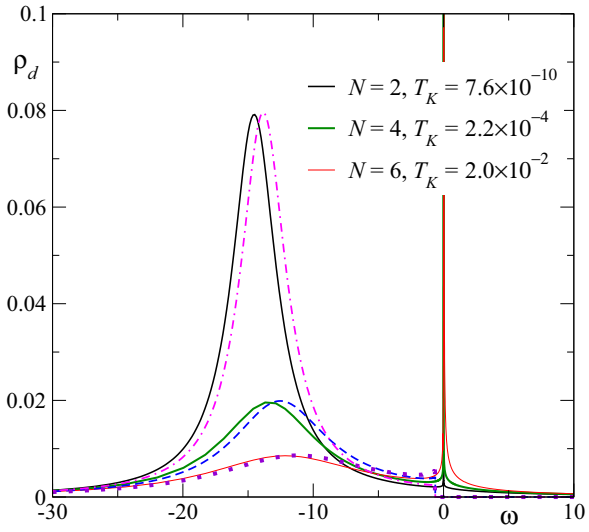

FIG. 2. Impurity spectral density calculated with the NCA (full lines) and variational wave function (dashed lines) for $E_d = -15\Delta$.

IV. WIDTH OF THE CHARGE-TRANSFER PEAK IN THE SU(4) IAM

In this section we show our results for Δ_{CT} as a function of E_d in the SU(4) case using NCA and DDMRG. For the NCA we used a constant density of unperturbed conduction states extending from $-D$ to D with $D = 100\Delta$. The assumptions made in DDMRG imply a semielliptical density of conduction states [45,77].

A. Temperature $T \to 0$

We discuss first the results at low temperature ($T = T_K/10$). Here T_K was chosen such that $G(T_K) = G_0/2$, where G_0 is the conductance of the system at $T = 0$ in the extreme Kondo limit in which the total occupancy is 1 (the maximum possible conductance of the system). Using Friedel sum rule [78,79] one has

$$G_0 = N\frac{e^2}{h}\sin^2\left(\frac{\pi}{N}\right). \tag{17}$$

In Fig. 2 we show the spectral density $\rho_m(\omega)$ obtained with the NCA in the Kondo regime ($-E_d \gg N\Delta$). It shows two peaks. The broad CT peak (which is the focus of this work) at E_d^{eff} (slightly larger than E_d) and the very narrow Kondo peak at the Fermi energy. Instead, for positive E_d (not shown) only the CT peak is present. We also show in the figure the result for $\rho_m^d(\omega)$ obtained using Eqs. (10), (4), and (6). One can see that there is a very good agreement between the NCA and variational calculations for the CT peak. We have verified that the CT peak in the empty orbital regime (not shown) looks identical to the noninteracting spectral density, as expected from the discussion of the previous section. Instead, in the

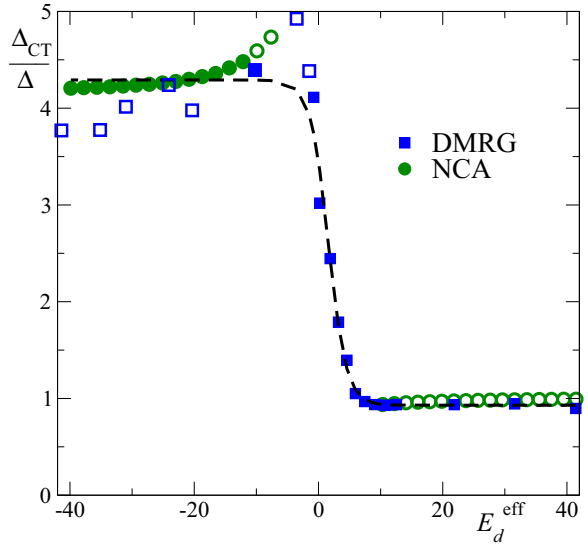

FIG. 3. Half width at half maximum of the charge transfer peak as a function of the effective on site energy using NCA (green circles) and DDMRG (blue squares). Dashed line is a fit of the filled symbols using Eq. (18).

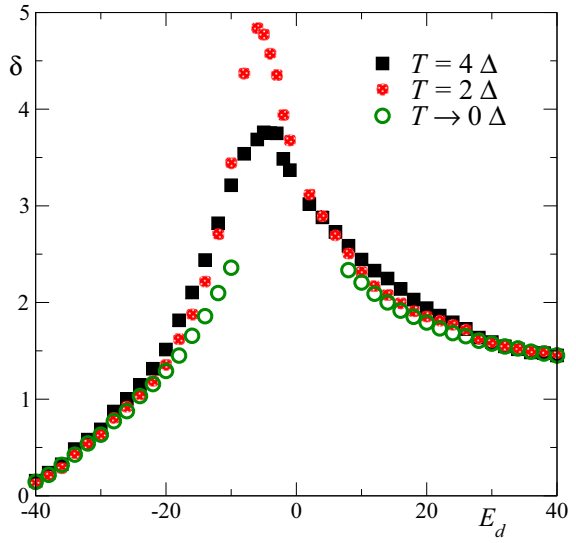

FIG. 4. Shift of the position of the CT peak as a function of on-site energy calculated with NCA for different temperatures T.

Kondo regime it is nearly four times broader and its maximum is sixteen times smaller.

We have repeated these calculations for several values of E_d. In the empty orbital regime, the peak has been fit with a Lorentzian with three parameters: the width identified with Δ_{CT}, the position E_d^{eff} and its weight w, which is the integral in energy of the Lorentzian. In the Kondo regime we used a similar fit with two Lorentzians, one for the CT peak and one for the Kondo peak. In the intermediate valence (IV) regime $|E_d^{eff}| \sim \Delta$, this procedure failed because in addition to the fact that the CT peak merges with a Kondo peak that becomes increasingly wider, the NCA fails and gives a self energy with a positive imaginary part. Thus, in this region, the DDMRG results are particularly useful.

In Fig. 3 we show the resulting Δ_{CT} as a function of E_d^{eff} using both techniques. The filled symbols denote the most reliable result between both. Due to the fact that the band is flat in the NCA and semielliptical in DDMRG (with a total width $2D = 200\Delta$), the resonant level width $2\Delta_{DDMRG}(\omega)$ is energy dependent in DDMRG and smaller than the corresponding width 2Δ within NCA, except for $\omega = 0$ where both widths are equal [45]. As a consequence for large $|E_d|$, a smaller Δ_{CT} is expected in the DDMRG calculation, as can be seen in the figure. In spite of the lack of NCA results near $E_d^{eff} = 0$, the results of both techniques indicate a rather sudden crossover from $\Delta_{CT} \sim 4\Delta$ to $\Delta_{CT} = \Delta$ at a slightly positive E_d^{eff}. In addition, there is an unexpected increase in Δ_{CT} for small negative E_d^{eff}. This might be due to the fact that the CT peak is deformed as it merges with the Kondo peak in this region.

For later use (Sec. VI), we also show in the figure a fit with the following function, which is an extension of that used in the SU(2) case

$$\frac{\Delta_{CT}}{\Delta} = a - b \tanh\left(\frac{E_d^{eff} - E_{IV}}{c\Delta}\right). \tag{18}$$

For general N one expects $a + b \simeq N$, $a - b \simeq 1$, so that this expression interpolates between the Kondo regime ($\Delta_{CT} \simeq N\Delta$ for $-E_d \gg N\Delta$) and the empty orbital one ($\Delta_{CT} = \Delta$ for $E_d \gg \Delta$) passing through the intermediate valence (IV) regime. From the fit we obtain $a = 2.61$, $b = 1.68$, $c = 2.90$, and $E_{IV} = 1.58\Delta$ for the effective level in the intermediate valence regime.

In Fig. 4 we show the shift $\delta = E_d^{eff} - E_d$ as a function of E_d. Approximate expressions of this shift were given based on functional renormalization group [32,44,76]. Generalizing Haldane's treatment to the SU(N) case [32] one obtains

$$\delta = \frac{N-1}{\pi}\Delta \ln\left(\frac{D}{C}\right), \tag{19}$$

where C is a low-energy cutoff. Haldane in his study of the SU(2) model used $C = \Delta$, while Filipone *et al.* have taken $C = |E_d|/\alpha$ with α of the order of 1 in the SU(4) case [76]. The NCA results in Fig. 4 seem to agree with a cutoff C of the order of the maximum between Δ and $|E_d|$. In the present paper the shift δ is larger than in similar calculations of Ref. [32] because of the larger value of D chosen ($D = 100$ here and $D = 10$ in Ref. [32]).

B. Finite temperatures

As the temperature increases, the above mentioned shortcomings of the NCA tend to disappear. For $T = 2\Delta$ the Kondo peak has disappeared (although some weak structure persists near $\omega = 0$ for small negative E_d^{eff}). Thus we have fit the CT peak using one Lorentzian. The results for Δ_{CT} as a function of E_d^{eff} are plotted in Fig. 5. For $T = 2\Delta$ still an upturn for slight negative E_d^{eff} is present, as for T near to 0 (see Fig. 3). For $T = 2\Delta$ this structure is greatly reduced and the fit using Eq. (18) improves. The parameters of the fit are for $T = 2\Delta$: $a = 2.81$, $b = 1.74$, $c = 2.51$, and $E_{IV} = -0.99\Delta$. For $T = 4\Delta$: $a = 2.82$, $b = 1.73$, $c = 6.26$, and $E_{IV} = -1.64\Delta$. Note that between $T = 2\Delta$ and $T = 4\Delta$, a broadening of crossover region between $\Delta_{CT} \sim 4\Delta$ and $\Delta_{CT} \sim \Delta$ by a factor larger

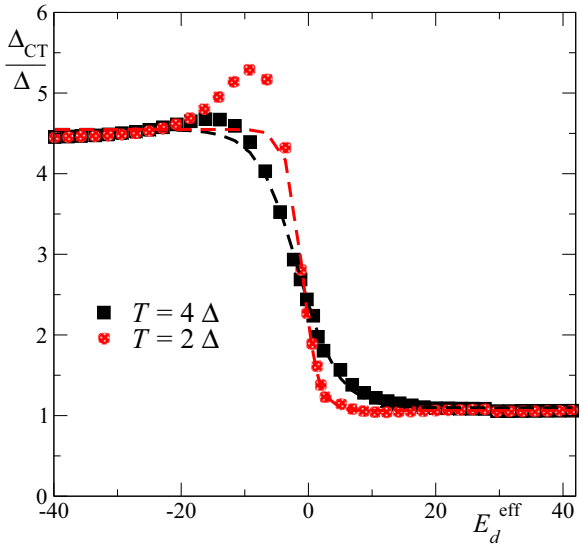

FIG. 5. Half width at half maximum of the charge transfer peak as a function of the effective on site energy using NCA at two different temperatures T. Dashed lines are fits using Eq. (18).

than two takes place. In addition, between very low T and $T = 2\Delta$, this region moves from slightly positive to slightly negative $E_d^{\rm eff}$.

V. OCCUPANCY FOR SU(2) AND SU(4)

To illustrate some of the effects of correlations, we show in Fig. 6 the total occupancy $n = \sum_m \langle n_m \rangle$ as a function of the energy level calculated from the integral of the pseudofermion density of states in the NCA [46]. This procedure is superior to the integral of the spectral density of the dot level and is free from the shortcomings of this density for positive E_d, like

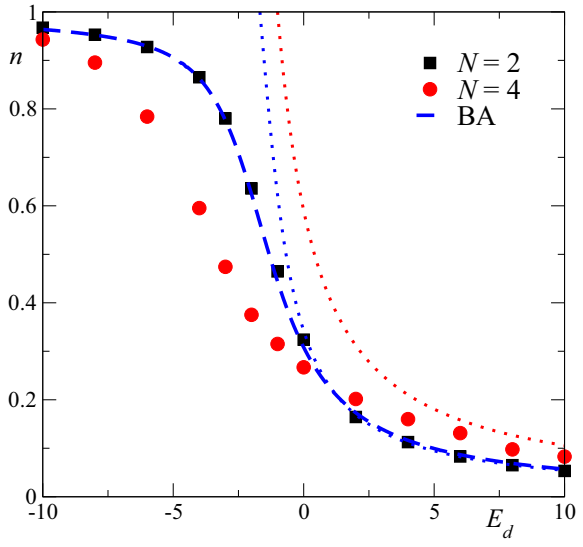

FIG. 6. Total occupancy as a function of on-site energy level calculated with NCA for the SU(N) IAM with $N = 2$ and 4. Dashed blue line corresponds to the Bethe ansatz (BA) result for $N = 2$ (see text). Dotted lines are the noninteracting results.

a spurious peak at the Fermi energy. This technical point is discussed in Ref. [80].

For $N = 2$ we include in the figure results obtained using the Bethe ansatz (BA) as described in Ref. [81]. These results were shifted to the left by a constant energy C to compensate by the Haldane shift and possible uncertainties in the position of E_d in the BA treatment. We have used $C = 1.67$. We also include in the figure the noninteracting results.

For $N = 2$ one can observe a very good agreement between NCA and BA results for all E_d. For positive E_d both results agree also with the $U = 0$ (noninteracting) case. However, for negative E_d, the effects of correlations become apparent. In particular for $U = 0$ and large negative E_d, $n = N$ for the SU(N) model, while for $U, -E_d \to \infty$, $n = 1$. This is due to the decreasing weight of the charge-transfer peak, discussed in Sec. III [see also Eq. (23) below].

The deviations from the noninteracting case are stronger in the SU(4) case. They are significant even for positive E_d. This is due in part to the larger Haldane shift in the SU(4) case. The fact that the increase in n with decreasing E_d is smoother than for the $N = 2$ case is due to the larger width of the charge-transfer peaks in the region of negative E_d.

VI. POSSIBLE EXPERIMENTS

A. Two dots independently connected to its own pair of leads

In the setup with two dots studied in Refs. [8–10], the dot $i = 1,2$ is connected to left and right ($\nu = L, R$) leads by couplings $\Delta_{\nu i}$ and all applied voltages and couplings can be controlled with high accuracy, For large enough repulsion between the dots [38], if $\Delta_{L1} + \Delta_{R1} = \Delta_{L2} + \Delta_{R2}$, and equal energy levels $E_{d2} = E_{d1}$, the system is in the SU(4) regime [10]. Even if the equality is not satisfied exactly, the SU(4) symmetry can be restored at low energies adjusting the difference $E_{d2} - E_{d1}$ [32,33]. In these conditions, if in addition the couplings of one dot are very asymmetric (say $\Delta_{L1} \ll \Delta_{R1}$), moving the bias voltage V_{L1} of the $L1$ lead, the resulting differential current through dot 1, dI_1/dV_{L1} just maps the spectral density of this dot (as in scanning tunneling spectroscopy) [39]. In this case, a marked asymmetry in the dI_1/dV_{L1} response for positive and negative E_{di} should be measured, as in Fig. (3). Previous nonequilibrium calculations show that if $\Delta_{L1} < \Delta_{R1}/9$, the resulting dI_1/dV_{L1} is very similar to the equilibrium spectral density for coupling $\Delta_{L1} + \Delta_{R1}$ and chemical potential corresponding to the right lead of dot 1.

B. Conductance through an SU(4) "impurity" including capacitance effects

Here we discuss an experiment like that of Könemann *et al.* [25] introduced in Sec. I, in which asymmetries with the sign of bias voltage V were observed in the widths and intensities of conductance peaks, but here we assume the QD or impurity described by the SU(4) IAM instead of the SU(2) one discussed previously [25,27]. Specifically, the interacting system, which we call impurity is coupled to two SU(4) interacting leads (left L and right R) with chemical potentials μ_ν and tunnel couplings Δ_ν ($\nu = L, R$), as described by the Hamiltonian Eq. (1).

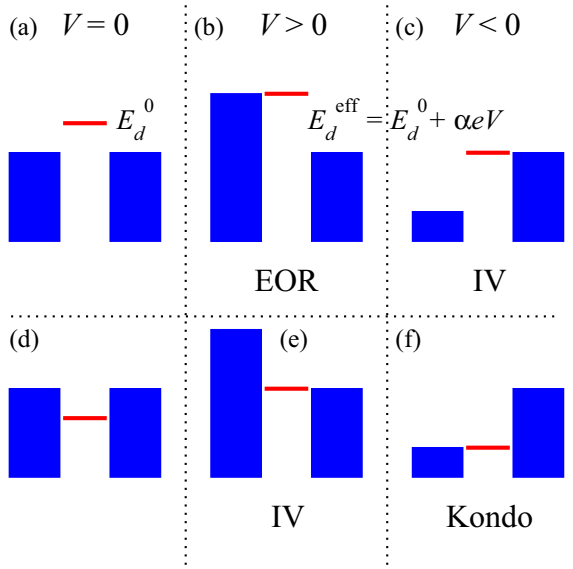

FIG. 7. Scheme of the Fermi level of both leads and the displacement of the dot level $E - d$ due to capacitance effects. The top (bottom) figures represent different situations for positive (negative) E_d^0. When the Fermi level of one of the leads coincides with E_d a peak in the conductance is observed. Assuming that the right lead is more strongly coupled to the dot, the system can be in Kondo, intermediate valence (IV), or empty orbital regime (EOR) as indicated.

We take the sign of the bias voltage in such a way that $\mu_L - \mu_R = eV$. Note that the interchange of right and left leads or electrons by holes is equivalent to a change of sign of V. In this section, we take the origin of energies at $\mu_R = 0$. The capacitance effects modify the energy necessary to add an electron to the dot with the lever arm parameter α (which depends on the source, drain, and gate capacitances) [25,26]. Usually $E_d = E_d^0 + \alpha eV$ is assumed, where $\alpha \sim 1/2$, so that E_d is displaced in approximately half the magnitude of $\mu_L - \mu_R$. Since the experimentally accessible quantity is $E_d^{\rm eff}$ and not E_d, we assume

$$E_d^{\rm eff} = E_d^0 + \alpha eV, \tag{20}$$

where E_d^0 is the effective dot level (the position of the CT peak) when $V = 0$ and α with $\leqslant \alpha \leqslant 1$ describes how the effective level is modified by the bias voltage. A scheme of how E_d is modified applying a bias voltage is presented in Fig. 7.

The current through the impurity is given by [82]

$$I = C \int d\omega \rho_m(\omega, V, E_d)[f_L(\omega) - f_R(\omega)],$$
$$C = \frac{4N\pi e \Delta_L \Delta_R}{h\Delta}, \tag{21}$$

where $N = 4$ in this section, $f_v(\omega) = f(\omega - \mu_v)$ is the Fermi distribution in each lead, with $f(\omega) = 1/(e^{\omega/kT} + 1)$, and $\rho_m(\omega, V, E_d)$ is the nonequilibrium spectral density of the impurity level with symmetry m, which depends on the voltage V explicitly and also implicitly through the voltage dependence of E_d [Eq. (20)]. The conductance is $G = dI/dV$.

As shown before [27], to observe the asymmetry in the peaks in $G(V)$ one needs asymmetric coupling to the leads. Therefore we assume $\Delta_R \gg \Delta_L$. It has been shown before

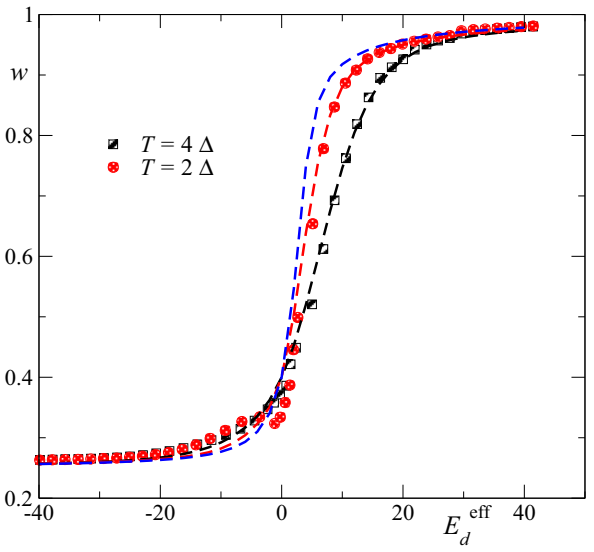

FIG. 8. Weight of the CT peak obtained from the fit of the NCA CT peak (circles and squares) and from Eqs. (23) and (24) (dashed lines) with $N = 4$ as a function of the effective impurity level for several temperatures T. Blue dashed line corresponds to $T = 0$.

[39] that for $\Delta_L \lesssim \Delta_R/9$, the spectral density at the dot practically coincides with the corresponding one with the dot at equilibrium with the right lead at chemical potential μ_R. This allows us to avoid a cumbersome nonequilibrium calculation.

To simplify the calculation further, we extend a phenomenological approach used before [27] to the present case and assume that the impurity spectral density near the CT peak can be approximated by

$$\rho_m(\omega) = \frac{(w\Delta_{\rm CT})/\pi}{\left(\omega - E_d^{\rm eff}\right)^2 + \Delta_{\rm CT}^2}, \tag{22}$$
$$w = 1 - \sum_{m' \neq m} \langle n_{m'} \rangle, \tag{23}$$

where $\langle n_m \rangle = \int d\omega \rho_m(\omega) f_R(\omega)$ is the occupation of the dot for symmetry m. The weight w is the probability that the site of the impurity is not occupied by electrons of symmetry different than m. This weight appears naturally in the atomic limit $V_q \to 0$ and was used in Hubbard-III [83] and similar [84,85] approximations to Hubbard and intermediate-valence models. Integrating Eq. (22), using Eq. (23) and SU(N) symmetry so that $\langle n_m \rangle$ is independent of m, one obtains a linear equation for $\langle n_m \rangle$. Solving it we obtain in general

$$\langle n_m \rangle = \frac{1 - 2\Psi_R}{(N+1) - 2(N-1)\Psi_R},$$
$$\Psi_v = \frac{1}{\pi} {\rm Im}\psi(\chi_v),$$
$$\chi_v = \frac{1}{2} + \frac{\Delta_{\rm CT} + i\left(E_d^{\rm eff} - \mu_v\right)}{2\pi T}, \tag{24}$$

where $\psi(x)$ is the digamma function.

In Fig. 8 we compare the weight obtained fitting the NCA results with those of the phenomenological approach given here. With the exception of the region in which both T and $E_d^{\rm eff}$ are near zero, we see that Eq. (22) reproduces well the

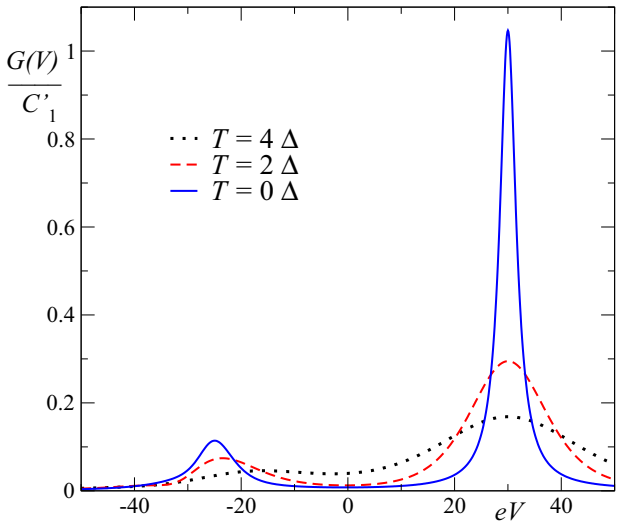

FIG. 9. Differential conductance for an SU(4) impurity as a function of bias voltage for asymmetric couplings $\Delta_R \gg \Delta_L$, capacitance ratio $\alpha = 1/2$, $E_d^0 = 15\Delta$ and several temperatures T. The constant $C_1' = eC/(2\pi\Delta)$.

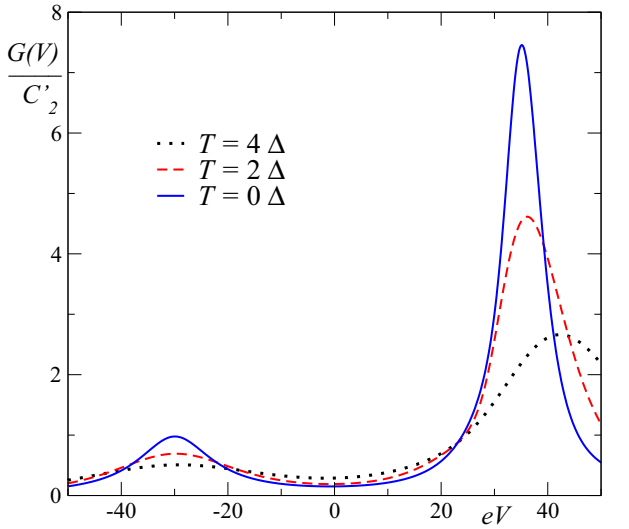

FIG. 10. Same as Fig. 9 for $E_d^0 = -15\Delta$. The constant $C_2' = eC/(32\pi\Delta)$.

NCA result. In particular for $|E_d^{\rm eff}| \gg \Delta$, Eq. (22) reproduces accurately the spectral density at the CT peak.

Replacing Eq. (22) in Eq. (21) gives the current

$$I = C[1 - (N-1)\langle n_m\rangle](\Psi_R - \Psi_L). \tag{25}$$

Differentiating this expression with respect to the voltage, using Eqs. (18), (20), and (24), we obtain for $N = 4$

$$\begin{aligned} G(V) &= C[(1 - 3\langle n_m\rangle)(\Psi_R' - \Psi_L') \\ &\quad + \frac{12\Psi_R'}{(5 - 6\Psi_R)^2}(\Psi_R - \Psi_L)], \\ \Psi_L' &= \frac{1}{2\pi^2 T}\mathrm{Im}\{\psi'(\chi_L)(i(\alpha-1) - \xi)\}, \\ \Psi_R' &= \frac{1}{2\pi^2 T}\mathrm{Im}\{\psi'(\chi_R)(i\alpha - \xi)\}, \\ \xi &= \frac{b\alpha}{c}\mathrm{Sech}\left[\frac{E_d^{\rm eff} - E_{\rm IV}}{c\Delta}\right]^2, \end{aligned} \tag{26}$$

and $\psi'(x)$ is the derivative of the digamma function.

The weak point in this approach is the use of the fit Eq. (18), which as can be seen in Figs. 3 and 5 fails near the intermediate valence regime ($E_d^{\rm eff} \sim 0$). However, this equation is accurate enough in the Kondo ($-E_d^{\rm eff} \gg N\Delta$) and empty orbital ($E_d^{\rm eff} \gg \Delta$) regimes.

In Fig. 9 we show the resulting conductance for E_d^0 slightly smaller than $E_d^{\rm eff}$ of the dotted line in Fig. 2. At $V = 0$, $E_d^{\rm eff}$ lies 15Δ at higher energy than $\mu_L = \mu_R = 0$. as V increases, a peak develops which reaches its maximum at $eV = 30\Delta$, for which $\mu_L = E_d^{\rm eff} = eV$. This configuration is similar to a scanning tunneling microscope (STM), for which the tip is very weakly coupled to the impurity. However, due to capacitance effects, the peak is broader by a factor $1/(1-\alpha)$ (two in the figure) [27], and the intensity at the maximum is near $(1-\alpha)eC/(\pi\Delta)$ as can be seen in the figure. This peak, which corresponds to the empty orbital regime, is accurately reproduced by our phenomenological approach. When a negative voltage is applied, $E_d^{\rm eff}$ decreases until for $eV = -30\Delta$ it reaches the value of $\mu_R = 0$. In this case, the system is in the intermediate-valence regime and for $T = 0$ our approach is not accurate because of the uncertainty in the width and weight of the CT in this region. From the spectral density, one would expect a peak nearly two times wider and a total weight reduced by a factor $2/5$, but also the strong dependence of $\Delta_{\rm CT}$ on V (through $E_d^{\rm eff}$) affects the shape. As expected, increasing the temperature has the effect of broadening both peaks, with more dramatic effects on the narrower one.

If the system is instead prepared starting from the Kondo regime $E_d^0 = -15\Delta$ (Fig. 10), at low temperatures one has the well known Kondo peak near zero bias [27]. Applying a positive V one reaches again the intermediate-valence regime for $eV = 30\Delta$ for which $E_d^{\rm eff} = \mu_R = 0$. Applying instead a negative voltage $eV \sim -30\Delta$, $\mu_L = eV$ again coincides with $E_d^{\rm eff}$ and a peak corresponding to a configuration similar to an STM one, but with a width increased by a factor $1/(1-\alpha)$ with respect to the spectral density, is obtained. Due to the increase of the width by a factor N and a decrease in the total weight of the peak by a factor $\sim 1/N$, the intensity at this relative maximum in $G(V)$ is near $(1-\alpha)eC/(N^2\Delta)$, as seen in the figure.

This peak corresponds to the Kondo regime and is well reproduced by our approach. Then we can anticipate that if an experiment with symmetric values of E_d^0 (with the same $|E_d^0|$ can be achieved, applying a gate voltage to the less coupled lead with the sign such that $|E_d^0|$ increases, in the case of negative E_d^0 (Kondo regime) the peak will be four times wider and nearly sixteen times less intense than for positive E_d^0 (empty orbital regime).

VII. SUMMARY AND DISCUSSION

We have calculated the width of the charge transfer peak in the infinite-U SU(4) Anderson model as a function of the impurity level E_d and for the general SU(N) case in the Kondo

regime $-E_d \gg N\Delta$, where Δ is half the resonant level width. While it is clear that in the empty orbital regime $E_d \gg \Delta$, the half width at half maximum of the charge transfer peak $\Delta_{\rm CT} = \Delta$, we obtain that in the Kondo regime $\Delta_{\rm CT} = N\Delta$ extending previous results for the SU(2) case [28,29]. The weight of the peak in the Kondo regime is reduced by a factor $\sim 1/N$ due to correlation effects, so that the maximum intensity is reduced by a factor $1/N^2$. The variational calculation presented in Sec. III provides a simple physical picture of the nontrivial effect of correlations in broadening the charge transfer peak in the Kondo regime.

The variational calculation of Sec. III suggests a simple interpretation of the width $\Delta_{\rm CT}$. For a peak below the Fermi level $\epsilon_F = 0$, the shape of the spectral density is defined by the spectral distribution of the state $|v>$ (not an eigenstate) obtained after annihilating one d_m electron [see the Eq. (9) for $\rho_m^d(\omega)$]. The hybridization term mixes this state with other states in which a d_m electron is created again. The number of ways M of adding this electron gives the number of bands that hybridize with $|v>$ and the width would be $\Delta_{\rm CT} = M\Delta$. For peaks above the Fermi energy the same argument would apply interchanging creation and annihilation. To check this idea and investigate the effects of finite U, we have run the DDMRG code for $E_d = -30$, and $U = 20$. We obtain peaks at $E_d + U$ and $E_d + 2U$ of width $\sim 3.2\Delta$ consistent with the expected $M = 3$. However, there is also an intense central peak which overlaps with the charge-transfer peak and renders it dangerous to draw definite conclusions.

To analyze general values of E_d, it is more useful to discuss it in terms of the position of the charge-transfer peak $E_d^{\rm eff}$ which incorporates a shift in the effective E_d discussed first by Haldane for the SU(2) case and more recently for the SU(4) case [32,76]. Our results for SU(4) symmetry suggest a rather abrupt decrease of $\Delta_{\rm CT}$ as $E_d^{\rm eff}$ increases from $\sim -\Delta$ to $\sim\Delta$, but our analysis at low temperature for small $|E_d^{\rm eff}|$ is complicated by the merge of the charge-transfer and Kondo peaks and limitations of our approaches.

The strong contrast between the charge-transfer peaks in the Kondo and empty-orbital regimes should be observable in experiment. This is discussed in Sec. VI. One possibility is a setup of two quantum dots [8–10], which can be tuned to prepare the system in a similar way as in scanning tunneling spectroscopies, with one quantum dot very weakly coupled to a lead to which a bias voltage is applied. Another possibility is to extend to an SU(4) system the experiment of Könemann *et al.*, in which strong asymmetries were observed in the width and magnitude of conductance peaks as a function of gate voltage for a quantum dot described by the SU(2) impurity Anderson model [25]. These experiments, in which also capacitance effects play a role [27], would display stronger asymmetries in the SU(4) case.

We hope that these results will encourage experimental work along these lines and be useful for the interpretation of Coulomb blockade peaks in conductance experiments. On the theoretical side, a deeper analysis of the change in $\Delta_{\rm CT}$ at zero temperature as $E_d^{\rm eff}$ crosses zero would be useful.

ACKNOWLEDGMENTS

J.F. and A.A.A. are sponsored by PIP 112-201101-00832 of CONICET and PICT2013-1045 of the ANPCyT. F.L. and C.G. acknowledge support from CONICET, through Project PIP No. 112-201201-00389.

[1] A. C. Hewson, *The Kondo Problem to Heavy Fermions* (Cambridge University Press, Cambridge, England, 1997).

[2] D. Goldhaber-Gordon, H. Shtrikman, D. Mahalu, D. Abusch-Magder, U. Meirav, and M. A. Kastner, Kondo effect in a single-electron transistor, Nature (London) **391**, 156 (1998).

[3] S. M. Cronenwett, T. H. Oosterkamp, and L. P. Kouwenhoven, A tunable kondo effect in quantum dots, Science **281**, 540 (1998).

[4] D. Goldhaber-Gordon, J. Göres, M. A. Kastner, H. Shtrikman, D. Mahalu, and U. Meirav, From the Kondo Regime to the Mixed-Valence Regime in a Single-Electron Transistor, Phys. Rev. Lett. **81**, 5225 (1998).

[5] W. G. van der Wiel, S. de Franceschi, T. Fujisawa, J. M. Elzerman, S. Tarucha, and L. P. Kowenhoven, The kondo effect in the unitary limit, Science **289**, 2105 (2000).

[6] M. Grobis, I. G. Rau, R. M. Potok, H. Shtrikman, and D. Goldhaber-Gordon, Universal Scaling in Nonequilibrium Transport through a Single Channel Kondo Dot, Phys. Rev. Lett. **100**, 246601 (2008).

[7] A. V. Kretinin, H. Shtrikman, D. Goldhaber-Gordon, M. Hanl, A. Weichselbaum, J. von Delft, T. Costi, and D. Mahalu, Spin-$\frac{1}{2}$ Kondo effect in an InAs nanowire quantum dot: Unitary limit, conductance scaling, and Zeeman splitting, Phys. Rev. B **84**, 245316 (2011).

[8] S. Amasha, A. J. Keller, I. G. Rau, A. Carmi, J. A. Katine, H. Shtrikman, Y. Oreg, and D. Goldhaber-Gordon, Pseudospin-Resolved Transport Spectroscopy of the Kondo Effect in a Double Quantum Dot, Phys. Rev. Lett. **110**, 046604 (2013).

[9] A. Hübel, K. Held, J. Weis, and K. v. Klitzing, Correlated Electron Tunneling through Two Separate Quantum Dot Systems with Strong Capacitive Interdot Coupling, Phys. Rev. Lett. **101**, 186804 (2008).

[10] A. J. Keller, S. Amasha, I. Weymann, C. P. Moca, I. G. Rau, J. A. Katine, H. Shtrikman, G. Zaránd, and D. Goldhaber-Gordon, Emergent SU(4) Kondo physics in a spincharge-entangled double quantum dot, Nat. Phys. **10**, 145 (2014).

[11] W. Liang, M. P. Shores, M. Bockrath, J. R. Long, and H. Park, Kondo resonance in a single-molecule transistor, Nature (London) **417**, 725 (2002).

[12] S. Kubatkin, A. Danilov, M. Hjort, J. Cornil, J. L. Brédas, N. Stuhr-Hansen, P. Hedegård, and Th. Bjørnholm, Single-electron transistor of a single organic molecule with access to several redox states, Nature (London) **425**, 698 (2003).

[13] L. H. Yu, Z. K. Keane, J. W. Ciszek, L. Cheng, J. M. Tour, T. Baruah, M. R. Pederson, and D. Natelson, Kondo Resonances and Anomalous Gate Dependence in the Electrical Conductivity of Single-Molecule Transistors, Phys. Rev. Lett. **95**, 256803 (2005).

[14] M. N. Leuenberger and E. R. Mucciolo, Berry-Phase Oscillations of the Kondo Effect in Single-Molecule Magnets, Phys. Rev. Lett. **97**, 126601 (2006).

[15] J. J. Parks, A. R. Champagne, G. R. Hutchison, S. Flores-Torres, H. D. Abruña, and D. C. Ralph, Tuning the Kondo Effect with a Mechanically Controllable Break Junction, Phys. Rev. Lett. **99**, 026601 (2007).

[16] N. Roch, S. Florens, V. Bouchiat, W. Wernsdorfer, and F. Balestro, Quantum phase transition in a single-molecule quantum dot, Nature (London) **453**, 633 (2008).

[17] G. D. Scott, Z. K. Keane, J. W. Ciszek, J. M. Tour, and D. Natelson, Universal scaling of nonequilibrium transport in the Kondo regime of single molecule devices, Phys. Rev. B **79**, 165413 (2009).

[18] J. J. Parks, A. R. Champagne, T. A. Costi, W. W. Shum, A. N. Pasupathy, E. Neuscamman, S. Flores-Torres, P. S. Cornaglia, A. A. Aligia, C. A. Balseiro, G. K.-L. Chan, H. D. Abruña, and D. C. Ralph, Mechanical control of spin states in spin-1 molecules and the underscreened kondo effect, Science **328**, 1370 (2010).

[19] G. D. Scott and D. Natelson, Kondo resonances in molecular devices, ACS Nano **4**, 3560 (2010).

[20] S. Florens, A, Freyn, N. Roch, W. Wernsdorfer, F. Balestro, P. Roura-Bas and A. A. Aligia, Universal transport signatures in two-electron molecular quantum dots: gate-tunable Hund's rule, underscreened Kondo effect and quantum phase transitions, J. Phys. Condens. Matter **23**, 243202 (2011) references therein.

[21] R. Vincent, S. Klyatskaya, M. Ruben, W. Wernsdorfer, and F. Balestro, Electronic read-out of a single nuclear spin using a molecular spin transistor, Nature (London) **488**, 357 (2012).

[22] P. Jarillo-Herrero, J. Kong, H. S. J. van der Zant, C. Dekker, L. P. Kouwenhoven, and S. De Franceschi, Electronic Transport Spectroscopy of Carbon Nanotubes in a Magnetic Field, Phys. Rev. Lett. **94**, 156802 (2005).

[23] A. Makarovski, A. Zhukov, J. Liu, and G. Finkelstein, SU(2) and SU(4) Kondo effects in carbon nanotube quantum dots, Phys. Rev. B **75**, 241407 (2007).

[24] F. B. Anders, D. E. Logan, M. R. Galpin, and G. Finkelstein, Zero-Bias Conductance in Carbon Nanotube Quantum Dots, Phys. Rev. Lett. **100**, 086809 (2008).

[25] J. Könemann, B. Kubala, J. König, and R. J. Haug, Tunneling resonances in quantum dots: Coulomb interaction modifies the width, Phys. Rev. B **73**, 033313 (2006).

[26] J. Park, Ph.D. thesis, University of California, 2003.

[27] A. A. Aligia, P. Roura-Bas, and S. Florens, Impact of capacitance and tunneling asymmetries on Coulomb blockade edges and Kondo peaks in nonequilibrium transport through molecular quantum dots, Phys. Rev. B **92**, 035404 (2015).

[28] Th. Pruschke and N. Grewe, The Anderson model with finite Coulomb repulsion, Z. Phys. B **74**, 439 (1989).

[29] D. E. Logan, M. P. Eastwood, and M. A. Tusch, A local moment approach to the Anderson model, J. Phys. Condens. Matter **10**, 2673 (1998).

[30] G. C. Tettamanzi, J. Verduijn, G. P. Lansbergen, M. Blaauboer, M. J. Calderón, R. Aguado, and S. Rogge, Magnetic-Field Probing of an SU(4) Kondo Resonance in a Single-Atom Transistor, Phys. Rev. Lett. **108**, 046803 (2012).

[31] G. P. Lansbergen, G. C. Tettamanzi, J. Verduijn, N. Collaert, S. Biesemans, M. Blaauboer, and S. Rogge, Tunable kondo effect in a single donor atom, Nano Lett. **10**, 455 (2010).

[32] L. Tosi, P. Roura-Bas, and A. A. Aligia, Restoring the SU(4) Kondo regime in a double quantum dot system, J. Phys.: Condens. Matter **27**, 335601 (2015).

[33] Y. Nishikawa, O. J. Curtin, A. C. Hewson, D. J. G. Crow, and J. Bauer, Conditions for observing emergent SU(4) symmetry in a double quantum dot, Phys. Rev. B **93**, 235115 (2016).

[34] C. A. Büsser, E. Vernek, P. Orellana, G. A. Lara, E. H. Kim, A. E. Feiguin, E. V. Anda, and G. B. Martins, Transport in carbon nanotubes: Two-level SU(2) regime reveals subtle competition between Kondo and intermediate valence states, Phys. Rev. B **83**, 125404 (2011).

[35] P. Roura-Bas, L. Tosi, A. A. Aligia, and K. Hallberg, Interplay between quantum interference and Kondo effects in nonequilibrium transport through nanoscopic systems, Phys. Rev. B **84**, 073406 (2011).

[36] C. A. Büsser, A. E. Feiguin, and G. B. Martins, Electrostatic control over polarized currents through the spin-orbital Kondo effect, Phys. Rev. B **85**, 241310(R) (2012).

[37] P. Roura-Bas, L. Tosi, A. A. Aligia, and P. S. Cornaglia, Thermopower of an SU(4) Kondo resonance under an SU(2) symmetry-breaking field, Phys. Rev. B **86**, 165106 (2012).

[38] Y. Nishikawa, A. C. Hewson, D. J. G. Crow, and J. Bauer, Analysis of low-energy response and possible emergent SU(4) Kondo state in a double quantum dot, Phys. Rev. B **88**, 245130 (2013).

[39] L. Tosi, P. Roura-Bas, and A. A. Aligia, Orbital Kondo spectroscopy in a double quantum dot system, Phys. Rev. B **88**, 235427 (2013).

[40] V. Lopes, R. A. Padilla, G. B. Martins, and E. V. Anda, SU(4)-SU(2) crossover and spin-filter properties of a double quantum dot nanosystem, Phys. Rev. B **95**, 245133 (2017).

[41] Y. Kleeorin and Y. Meir, Abrupt disappearance and re-emergence of the SU(4) and SU(2) Kondo effects due to population inversion, Phys. Rev. B **96**, 045118 (2017).

[42] C. M. Varma and Y. Yafet, Magnetic susceptibility of mixed-valence rare-earth compounds, Phys. Rev. B **13**, 2950 (1976).

[43] O. Gunnarsson and K. Schönhammer, Photoemission from Ce Compounds: Exact Model Calculation in the Limit of Large Degeneracy, Phys. Rev. Lett. **50**, 604 (1983).

[44] F. D. M. Haldane, Scaling Theory of the Asymmetric Anderson Model, Phys. Rev. Lett. **40**, 416 (1978).

[45] In the DDMRG calculations the two chains were attached to two semi-infinite chains of conducting electrons described by a tight binding Hamiltonian with hopping $t = D/2$. In this case $\Delta(\omega)$ has an energy dependence given by $\Delta(\omega) = \Delta[1 - (\omega/D)^2$ [77]. For $D = 100$ as we have taken, this dependence is weak. For example $\Delta(\omega) = 0.92\Delta$ for $|\omega = 40|$.

[46] N. E. Bickers, Review of techniques in the large-N expansion for dilute magnetic alloys, Rev. Mod. Phys. **59**, 845 (1987).

[47] J. Kroha and P. Wölfle, Fermi and non-fermi liquid behavior in quantum impurity systems: Conserving slave boson theory, Acta Phys. Pol. B **29**, 3781 (1998).

[48] R. Žitko, Quantitative determination of the discretization and truncation errors in numerical renormalization-group calculations of spectral functions, Phys. Rev. B **84**, 085142 (2011).

[49] L. Vaugier, A. A. Aligia and A. M. Lobos, Spectral density of an interacting dot coupled indirectly to conducting leads, Phys. Rev. B **76**, 165112 (2007).

[50] J. Fernández, A. A. Aligia, P. Roura-Bas, and J. A. Andrade, Kondo temperature when the Fermi level is near a step in the conduction density of states, Phys. Rev. B **95**, 045143 (2017).

[51] N. S. Wingreen and Y. Meir, Anderson model out of equilibrium: Noncrossing-approximation approach to transport through a quantum dot, Phys. Rev. B **49**, 11040 (1994).

[52] F. Reinert, D. Ehm, S. Schmidt, G. Nicolay, S. Hüfner, J. Kroha, O. Trovarelli, and C. Geibel, Temperature Dependence of the Kondo Resonance and Its Satellites in $CeCu_2Si_2$, Phys. Rev. Lett. **87**, 106401 (2001).

[53] D. Ehm, S. Hüfner, F. Reinert, J. Kroha, P. Wölfle, O. Stockert, C. Geibel, and H. v. Löhneysen, High-resolution photoemission study on low-TK Ce systems: Kondo resonance, crystal field structures, and their temperature dependence, Phys. Rev. B **76**, 045117 (2007).

[54] Roura-Bas, L. Tosi, and A. A. Aligia, Nonequilibrium transport through magnetic vibrating molecules, Phys. Rev. B **87**, 195136 (2013).

[55] P. Roura-Bas, L. Tosi, and A. A. Aligia, Replicas of the Kondo peak due to electron-vibration interaction in molecular transport properties, Phys. Rev. B **93**, 115139 (2016).

[56] S. Di Napoli, P. Roura-Bas, A. Weichselbaum, and A. A. Aligia, Non-Fermi-liquid behavior in nonequilibrium transport through Co-doped Au chains connected to fourfold symmetric leads, Phys. Rev. B **90**, 125149 (2014).

[57] P. Roura Bas and A. A. Aligia, Nonequilibrium transport through a singlet-triplet Anderson impurity, Phys. Rev. B **80**, 035308 (2009); J. Phys. Condens. Matt. **22**, 025602 (2010).

[58] A. C. Hewson, J. Bauer, and A. Oguri, Non-equilibrium differential conductance through a quantum dot in a magnetic field, J. Phys.: Condens. Matter **17**, 5413 (2005), and references therein.

[59] A. A. Aligia, Nonequilibrium self-energies, Ng approach, and heat current of a nanodevice for small bias voltage and temperature, Phys. Rev. B **89**, 125405 (2014), and references therein.

[60] A. A. Aligia, Comment on "The renormalized superperturbation theory (rSPT) approach to the Anderson model in and out of equilibrium", arXiv:1706.06029.

[61] M. A. Romero, S. C. Gómez-Carrillo, P. G. Bolcatto, and E. C. Goldberg, Spin fluctuation effects on the conductance through a single Pd atom contact, J. Phys. Condens. Matter **21**, 215602 (2009).

[62] R. Van Roermund, S. Y. Shiau, and M. Lavagna, Anderson model out of equilibrium: Decoherence effects in transport through a quantum dot, Phys. Rev. B **81**, 165115 (2010).

[63] M. A. Romero, F. Flores, and E. C. Goldberg, Effective treatment of charge and spin fluctuations in dynamical and static atom-surface interactions, Phys. Rev. B **80**, 235427 (2009).

[64] T. D. Kühner and S. R. White, Dynamical correlation functions using the density matrix renormalization group, Phys. Rev. B **60**, 335 (1999).

[65] T. Hövelborn, Diploma thesis, Bonn/Köln, 2000, available at www.thp.uni-koeln.de/∼gu.

[66] R. W. Freund, A transpose-free quasi-minimal residual algorithm for non-hermitian linear systems, SIAM J. Sci. Comput. **14**, 470 (1993).

[67] E. Jeckelmann, A transpose-free quasi-minimal residual algorithm for non-hermitian linear systems, Phys. Rev. B **66**, 045114 (2002).

[68] A. Nocera and G. Alvarez, Spectral functions with the density matrix renormalization group: Krylov-space approach for correction vectors, Phys. Rev. E **94**, 053308 (2016).

[69] F. Gebhard, E. Jeckelmann, S. Mahlert, S. Nishimoto, and R. M. Noack, Fourth-order perturbation theory for the half-filled Hubbard model in infinite dimensions, Eur. Phys. J. B **36**, 491 (2003).

[70] T. Ulbricht and P. Schmitteckert, Tracking spin and charge with spectroscopy in spin-polarised 1D systems, Europhys. Lett. **89**, 47001 (2010).

[71] A. Weichselbaum, F. Verstraete, U. Schollwöck, J. I. Cirac, and J. von Delft, Variational matrix-product-state approach to quantum impurity models, Phys. Rev. B **80**, 165117 (2009).

[72] S. Nishimoto and E. Jeckelmann, Density-matrix renormalization group approach to quantum impurity problems, J. Phys.: Condens. Matter **16**, 613 (2004).

[73] C. Raas and S. G. Uhrig, Spectral densities from dynamic density-matrix renormalization, Eur. Phys. J. B **45**, 293 (2005).

[74] C. Raas, G. S. Uhrig, and F. B. Anders, High energy dynamics of the single impurity anderson model, Phys. Rev. B **69**, 041102 (2004).

[75] M. Paech and E. Jeckelmann, Blind deconvolution of density-matrix renormalization-group spectra, Phys. Rev. B **89**, 195101 (2014).

[76] M. Filippone, C. P. Moca, G. Zaránd, and C. Mora, Kondo temperature of SU(4) symmetric quantum dots, Phys. Rev. B **90**, 121406(R) (2014).

[77] A. A. Aligia and C. R. Proetto, Kondo and anti-Kondo resonances in transport through nanoscale devices, Phys. Rev. B **65**, 165305 (2002).

[78] David C. Langreth, Friedel sum rule for anderson's model of localized impurity states, Phys. Rev. **150**, 516 (1966).

[79] A. Yoshimori and A. Zawadowski, Restricted Friedel sum rules and Korringa relations as consequences of conservation laws, J. Phys. C **15**, 5241 (1982).

[80] T. A. Costi, J. Kroha, and P. Wölfle, Spectral properties of the Anderson impurity model: Comparison of numerical-renormalization-group and noncrossing-approximation results, Phys. Rev. B **53**, 1850 (1996).

[81] I. J. Hamad, P. Roura-Bas, A. A. Aligia, and E. V. Anda, Self-consistent hybridization expansions for static properties of the Anderson impurity model, Physica Status Solidi (b) **253**, 478 (2015).

[82] Y. Meir and N. S. Wingreen, Landauer Formula for the Current Through an Interacting Electron Region, Phys. Rev. Lett. **68**, 2512 (1992).

[83] J. Hubbard, Electron correlations in narrow energy bands III. An improved solution, Proc. Roy. Soc. A **281**, 401 (1964).

[84] H. J. Leder and G. Czycholl, Self-consistent alloy treatment of the periodic anderson model: Susceptibility and specific heat of intermediate valence compounds, Z. Phys. B. **35**, 7 (1979).

[85] A. A. Aligia and B. Alascio, Dynamical magnetic susceptibility of intermediate valence Tm systems, J. Magn. Magn. Mat. **46**, 321 (1985).